




The charm-quark contribution to light-by-light scattering in the muon ($g - 2$) from lattice QCD

En-Hung Chao¹, Renwick J. Hudspith¹, Antoine Gérardin², Jeremy R. Green³, Harvey B. Meyer^{1,4,5,a} 

¹ PRISMA+ Cluster of Excellence, Institut für Kernphysik, Johannes Gutenberg-Universität Mainz, 55099 Mainz, Germany

² Aix Marseille Univ, Université de Toulon, CNRS, CPT, Marseille, France

³ School of Mathematics and Hamilton Mathematics Institute, Trinity College, Dublin 2, Ireland

⁴ Helmholtz Institut Mainz, Staudingerweg 18, 55128 Mainz, Germany

⁵ GSI Helmholtzzentrum für Schwerionenforschung, Darmstadt, Germany

Received: 2 May 2022 / Accepted: 6 July 2022 / Published online: 2 August 2022
© The Author(s) 2022

Abstract We compute the hadronic light-by-light scattering contribution to the muon $g-2$ from the charm quark using lattice QCD. The calculation is performed on ensembles generated with dynamical (u , d , s) quarks at the $SU(3)_F$ symmetric point with degenerate pion and kaon masses of around 415 MeV. It includes the connected charm contribution, as well as the leading disconnected Wick contraction, involving the correlation between a charm and a light-quark loop. Cutoff effects turn out to be sizeable, which leads us to use lighter-than-physical charm masses, to employ a broad range of lattice spacings reaching down to 0.039 fm and to perform a combined charm-mass and continuum extrapolation. We use the η_c meson to define the physical charm-mass point and obtain a final value of $a_\mu^{\text{HLbL},c} = (2.8 \pm 0.5) \times 10^{-11}$, whose uncertainty is dominated by the systematics of the extrapolation. Our result is consistent with the estimate based on a simple charm-quark loop, whilst being free of any perturbative scheme dependence on the charm mass. The mixed charm–light disconnected contraction contributes a small negative amount to the final value.

1 Introduction

The anomalous magnetic moment of the muon, $a_\mu \equiv (g - 2)_\mu/2$, is one of the most precisely measured quantities in fundamental physics. Currently, the experimental world average [1,2] and the theoretical evaluation of the 2020 White Paper (WP) [3] based on the Standard Model (SM) of particle physics are in tension at the 4.2σ level. The theory uncertainties are entirely dominated by the hadronic contributions. Surprisingly, a lattice-QCD based calculation [4] of the leading hadronic contribution finds a larger value than

the dispersion-theory based estimate of the WP, which would bring the overall theory prediction into far better agreement with the experimental value of a_μ . Thus it will be vital to resolve the tension between the different determinations of the leading hadronic contribution in order to strengthen the unique test of the SM offered by the anomalous magnetic moment of the muon.

A subleading hadronic contribution to a_μ , the hadronic light-by-light (HLbL) contribution, also contributes sizeably to the error budget of the SM prediction. The HLbL contribution is significantly more complex to evaluate than the leading hadronic contribution; however, because it is suppressed by an additional power of the fine-structure constant α , it only needs to be determined at the ten percent level. In the past decade, the HLbL contribution, too, has been evaluated using either dispersive methods [5], assisted by short-distance constraints and hadron structure input [6–18], or lattice QCD. In this case, good agreement is found between the dispersive [3] and the two lattice evaluations [19,20] within the quoted uncertainties.

One missing ingredient in the otherwise complete HLbL calculation of [20] is the contribution of the charm quark. The present paper addresses this missing contribution. Since the charm quark is much heavier than the muon, on general grounds [21–23] one expects this contribution to be in a regime where it is roughly proportional to m_μ^2/m_c^2 . In phenomenological estimates, it has been evaluated using the prediction based on quantum electrodynamics (QED), amended for the appropriate charge and colour factors [24]. We quote the value and uncertainty from the 2020 White Paper (WP) [3],

$$a_\mu^{\text{HLbL},c}(\text{WP}) = (3 \pm 1) \times 10^{-11}. \quad (1)$$

^a e-mail: meyerh@uni-mainz.de (corresponding author)

While the central value comes from evaluating the QED-like quark-loop, the uncertainty has been estimated conservatively based on the size of the η_c pole contribution [12]. Since the WP appeared, the leading radiative correction to a massless quark loop has also been computed [25]. The main goal of this paper is thus to test the prediction (1) using lattice QCD, in case a qualitative effect might have been missed. Certainly, this contribution is small compared to the overall uncertainty 43×10^{-11} of the WP prediction for a_μ , however the other uncertainties are also expected to shrink, especially if the issues in the leading hadronic contribution can be resolved.

Our second motivation for addressing the charm HLbL contribution from first principles is to answer the qualitative question whether approximating this contribution via a simple quark loop is adequate. In lattice QCD, the calculation involves computing charm propagators on an ensemble of non-perturbative background SU(3) gauge fields. If the simple quark-loop picture is approximately correct, the details of this gauge field should not matter much, and the charm propagators can be replaced by free Dirac propagators. In this case, the sensitivity to the sea quarks enters (at the earliest) at quadratic order in $\alpha_s(m_c)$, the strong coupling constant at the scale of the charm mass. It is largely for this reason that we will focus on the SU(3)_f-symmetric mass point with $m_\pi = m_K \simeq 415$ MeV, enabling us to reach sufficiently fine lattices at a moderate computational cost.

A further aspect of the quark-loop picture is that the various disconnected diagrams entering the HLbL amplitude are expected to be small. In contrast, if the η_c pole exchange or D meson loops played a sizeable role in the charm-quark contribution, the leading disconnected charm contribution, consisting of a charm loop and a light-quark loop, each attached to two electromagnetic currents, would be sizeable (in analogy to the analyses in [26] and Appendix A of Ref. [20] for the three-flavour case). We recall that for the light quarks, individual mesons, especially the pseudoscalars π^0 , η , η' , contribute substantially to a_μ^{HLbL} , even at the aforementioned SU(3)_f-symmetric point [27]. In lattice QCD, we can quantitatively test the relevance of the disconnected contributions.

This paper is organized as follows. We describe our lattice setup, the tuning of the charm quark mass and our specific representation of a_μ^{HLbL} in Sect. 2. Section 3 provides some basic theory expectations concerning the connected and leading disconnected contributions involving a charm quark. Section 4 presents our lattice results on the connected contribution for a sequence of increasing charm-quark masses, and Sect. 5 contains our results at the target charm mass for the leading topology of disconnected diagrams. We provide our final result and conclude in Sect. 6. Appendix A describes a test of our methods at a heavy quark mass in lattice QED, while Appendix B contains tables of results for the connected

charm contribution on individual ensembles and Appendix C a representative set of fit results.

2 Lattice setup

We have performed lattice-QCD calculations on gauge ensembles provided by the Coordinated Lattice Simulations (CLS) initiative [28], which have been generated using three flavours of non-perturbatively $O(a)$ -improved Wilson-clover fermions and with the tree-level-improved Lüscher–Weisz gauge action. As in Ref. [27], where we computed the (u, d, s) quark contribution, we consider only ensembles realizing exact SU(3)_f-symmetry. On these ensembles, the mass of the octet of light pseudoscalar mesons is approximately 415 MeV. The parameters of these ensembles, which correspond to six different values of the lattice spacing, are summarized in Table 1.

2.1 Calibrating the charm mass and current

The connected contribution to a_μ^{HLbL} and the two-point correlation function of $\bar{c}\gamma_5 c$ were computed on all ensembles of Table 1 for several (5 or 7) values of the charm-quark bare subtracted mass $am_c = (\kappa_c^{-1} - \kappa_{\text{crit}}^{-1})/2$, with values of κ_c chosen to interpolate between the physical strange and charm hopping parameters. A determination of the latter is available from Ref. [30], obtained by tuning the D_s meson mass to its physical value. For the (dominant) connected contribution however, we choose the physical charm-mass point as the one defined by the physical value of the η_c meson mass. When we determine the η_c mass, we do not include the disconnected diagram in the two-point function of the charm pseudoscalar density. This procedure corresponds to using the operator $\bar{c}'\gamma_5 c$ ($am_{c'} = am_c$), where the degenerate quark flavours c and c' are both treated at the partially-quenched level. It should be noted that the tuning of Ref. [30] by the D_s yields a heavier-than-physical η_c meson at our SU(3)_f-symmetric point. This comes from the quark masses at the latter point being lighter than the physical strange quark, and a D_s -tuning *de facto* absorbs this effect into the charm-quark mass [31].

The reason for using lighter-than-physical charm quark masses is that we expect discretisation effects to become more and more significant when the charm mass increases. For a rough estimate of the typical size of discretisation effects, [31] found that the effective speed of light (as defined by the dispersion relation of a meson) for physical-mass charm quarks at worst deviates from unity by 20% in our setup.

The finite renormalisation factor $Z_V^c(g_0, am_c)$ for the local charm current $\bar{c}\gamma_\mu c$ was determined by requiring the corresponding charge of the ground-state meson created when $\bar{c}'\gamma_5 c$ acts on the vacuum to be unity. The meson corre-

Table 1 The $SU(3)_f$ -symmetric ensembles used in this work. Each ensemble is parametrized by the gauge coupling parameter $\beta \equiv 6/g_0^2$, the (u, d, s) -quark hopping parameter κ , the lattice size, and the temporal boundary condition. The lattice spacings a were determined in Ref. [29], apart from A653 and J500, where the lattice spacings were esti-

mated from the ratio of the Wilson flow parameter t_0 ; the errors on the lattice spacing for these two ensembles (in bold) are simply estimated by scaling of the total error of the neighboring lattice spacings. Their pion masses (marked with asterisk) have been measured independently for this work

Label	β	κ	$L^3 \times L_T$	Temporal B.Cs	a (fm)	$m_{\pi,K,\eta}$ (MeV)
A653	3.34	0.1365716	$24^3 \times 48$	Periodic	0.09930(122)	413(5)*
H101	3.40	0.13675962	$32^3 \times 96$	Open	0.08636(98)(40)	418(5)
B450	3.46	0.13689	$32^3 \times 64$	Periodic	0.07634(92)(31)	417(5)
N202	3.55	0.137000	$48^3 \times 128$	Open	0.06426(74)(17)	412(5)
N300	3.70	0.137000	$48^3 \times 128$	Open	0.04981(56)(10)	421(5)
J500	3.85	0.136852	$64^3 \times 192$	Open	0.03910(46)	413(5)*

lators were computed using $Z_2 \times Z_2$ stochastic wall sources [32, 33]. The quark-mass dependence of $Z_V^c(g_0, am_c)$ is quite strong, especially at coarse lattice spacings. Since this factor enters to the third power into our final result, we determine it directly for every one of the bare quark-mass values. This is the same procedure that was implemented for the charm renormalisation in [30].¹

2.2 Computing the charm contribution to a_μ^{HLbL}

We apply the formalism described and used in [20, 27] and therefore only recall the main aspects. The starting point of our calculation is the master formula²

$$a_\mu^{\text{HLbL}} = \int_0^\infty d|y| f(|y|),$$

$$f(|y|) = \frac{m_\mu e^6}{3} 2\pi^2 |y|^3 \int_x \tilde{\mathcal{L}}_{[\rho,\sigma];\mu\nu\lambda}(x, y) i\hat{\Pi}_{\rho;\mu\nu\lambda\sigma}(x, y).$$

(2)

Here $e^2/(4\pi) = \alpha_{\text{QED}}$ is the fine-structure constant and m_μ the muon mass. The QED kernel $\tilde{\mathcal{L}}$ has been computed in the continuum [34] and represents the contributions of the photon and muon propagators and vertices in the diagrams of Fig. 1. There is a lot of freedom to alter the kernel without changing a_μ^{HLbL} in the continuum and in infinite volume. Specifically, we use the kernel $\tilde{\mathcal{L}}^{(\Lambda)}$ defined in [27] with $\Lambda = 0.40$ throughout.³ The tensor $i\hat{\Pi}$ is a Euclidean hadronic four-point function with one of its vertices weighted linearly in one of its coordinates,

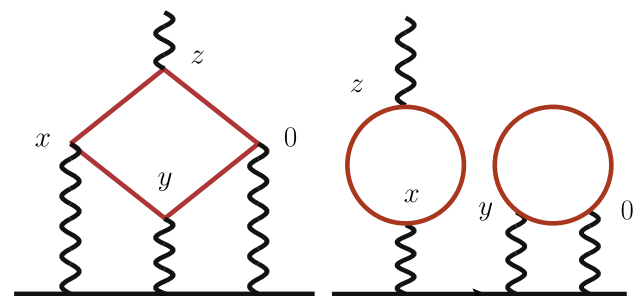


Fig. 1 The fully connected charm contribution (left) and the (2+2) Wick contraction (right, with at least one loop corresponding to a charm quark) are the two Wick contractions computed in this work

$$i\hat{\Pi}_{\rho;\mu\nu\lambda\sigma}(x, y) = - \int_z z_\rho \left\langle j_\mu(x) j_\nu(y) j_\sigma(z) j_\lambda(0) \right\rangle_{\text{QCD}}.$$

(3)

The field $j_\mu(x)$ appearing above is the hadronic component of the electromagnetic current,

$$j_\mu(x) = \sum_f \mathcal{Q}_f (\bar{q}_f \gamma_\mu q_f)(x).$$

(4)

Here we focus on the contributions involving the charm current, $\bar{c}\gamma_\mu c$. The QCD four-point function receives contributions from five classes of Wick contractions. First, we will focus on the fully-connected charm contribution, which involves four charm currents; for this contribution, we apply Eq. (7) of Ref. [20] with the flavour index set to charm, $j := c$. Second, we will consider the disconnected contributions involving two quark loops, each of which containing two vector vertices, with either one or both loops consisting of charm propagators. Here we apply Eq. (11) of Ref. [20] with the flavour indices i, j running over $\{u, d, s, c\}$ under the constraint that at least one of them take the value c . The connected and (leading) disconnected contributions are illustrated in Fig. 1.

¹ In that paper, the Z_V^c values quoted in its Appendix A are erroneously described as stemming from the charm number of the D_s meson.

² See however the text below Eq. (4) for references to the precise formulae used in the present calculation.

³ We have also investigated the effect of choosing $\Lambda = 0$ and found it to make very little difference.

3 Theory expectations

The simplest prediction for the light-by-light contribution of a heavy ‘charm’ quark to $10^{11}a_\mu$ relies on the analytic QED result originally applied to the τ lepton loop [35,36]. Taking into account the colour factor $N_c = 3$ and the charge factor $(2/3)^4$, it is given by the function

$$h(m_Q) = 5.10382 \frac{1}{\hat{m}_Q^2} + \left(-0.176225 - 0.0567645 \log(\hat{m}_Q^2) - 0.00459931 \log^2(\hat{m}_Q^2) \right) \frac{1}{\hat{m}_Q^4}, \tag{5}$$

with \hat{m}_Q is the heavy-quark mass in GeV. Already by $m_Q = 0.75$ GeV, the $O(m_Q^{-4})$ terms only represent a reduction of the leading term by five percent. These terms certainly represent a small correction for m_Q around the physical charm mass. Here we have dropped known higher-order terms in $1/m_Q$. We will take the function $h(m_Q)$ as a baseline for comparison with our lattice results for the fully connected charm contribution.

For the (2+2) disconnected contribution involving one charm and one light-quark loop, it is less straightforward to make a ‘baseline’ prediction. The scalar-QED prediction for the contribution to a_μ^{HLbL} of the D^\pm meson loop is -0.33×10^{-11} [36], to be roughly doubled in order to include the D_s loop. Taking into account the charge factor of $2 \cdot 3 \cdot Q_c^2(Q_u^2 + Q_d^2 + Q_s^2) = \frac{144}{81}$ relevant for the charm–light (2+2) contribution (see [20], Appendix A⁴), one arrives at the prediction of $a_\mu^{2+2;lc} = -0.58 \times 10^{-11}$ when treating the D^+ , D^0 , D_s meson loops within scalar QED.⁵ The absolute value of this prediction is surely an overestimate, given that electromagnetic form factors of the D mesons should suppress this prediction substantially: in the case of the pion loop, the suppression factor is almost three, and for the kaon almost ten [3,36]. All in all, these considerations finally lead us to expect an order of magnitude of $(-0.3 \pm 0.3) \times 10^{-11}$.

In addition to the short-distance effect estimated above, the charm–light disconnected diagrams also involve a longer-distance contribution, whose size it is useful to estimate by theory arguments, given the difficulty of measuring the correlation function in the infrared. The intuitive idea is that the heavy-quark loop shrinks almost to a point in coordinate-space,⁶ acting effectively like a local gauge-invariant gluonic operator from the point of view of the ‘low-energy effective theory’, which is QCD with (u, d, s) quarks. This picture

⁴ The analysis of this reference can be applied here due to the u, d, s quarks being degenerate and the charm quark being quenched.

⁵ Note that the D^0 loop contributes to $a_\mu^{2+2;lc}$, even though at the scalar-QED level it does not contribute to a_μ^{HLbL} , due to it cancelling between different topologies.

⁶ This picture holds when the vertices of the light-quark loop are at a distance much greater than $(2m_c)^{-1}$ from the charm loop.

can be formalized by writing an effective Lagrangian for the effective coupling induced between two photons and gluonic fields, much as in the classic work of Euler and Heisenberg [37]. This effective Lagrangian $\mathcal{L}_{2\gamma 2g}^{(c)}$ has been calculated long ago [38]; each term of the Lagrangian contains two photonic and two gluonic field strength tensors. From here, one infers the operator equation

$$Q_c^2 T\{(\bar{c}\gamma^\mu c)(x) (\bar{c}\gamma^\mu c)(y)\} = \frac{1}{e^2} \frac{\delta^2}{\delta A_\mu(x) \delta A_\nu(y)} \int d^4w \mathcal{L}_{2\gamma 2g}^{(c)}(w), \tag{6}$$

A_μ being the photon field, which shows that the charm loop acts at low energies like a set of gluonic operators such as $\alpha_s G_{\mu\nu}^a G_{\mu\nu}^a$ or $\alpha_s G_{\mu\nu}^a \tilde{G}_{\mu\nu}^a$. The main observation is that, on dimensional grounds, the effective Lagrangian is overall multiplied by a $1/m_c^4$ factor, indicating a strong suppression.

The argument above shows that a light flavour-singlet meson such as the scalar f_0 or the pseudoscalar η' can propagate between the charm loop and the light-quark loop, albeit with a very suppressed coupling to the charm loop. To get an estimate of this contribution, which is long-range in comparison to the length-scale $(2m_c)^{-1}$, we use Eq. (6) to find out roughly how much the charm part of the electromagnetic current by itself contributes to the η' transition form factor (TFF). Note that this contribution is independent of the photon virtualities, as long as these are small. Using the estimate $\langle 0 | \alpha_s G \tilde{G} | \eta' \rangle \approx 0.5 \text{ GeV}^3$ based on Ref. [39], while the TFF normalisation amounts to $|\mathcal{F}_{\eta'\gamma\gamma}(0, 0)| \simeq 0.34 \text{ GeV}^{-1}$ (see for instance [40]), we obtain a contribution of about $8 \times 10^{-4} \text{ GeV}^{-1}$ to $\mathcal{F}_{\eta'\gamma\gamma}$ from the charm current. Since the η' exchange contributes about 14.5×10^{-11} to a_μ^{HLbL} [3], proportionally to its TFF at each end of η' propagator, we arrive at the order-of-magnitude estimate of 0.01×10^{-11} for the contribution to a_μ^{HLbL} of the η' in the (2+2) charm–light diagrams. Even with a potential logarithmic enhancement [41], this is much smaller than our final uncertainty and cannot presently be resolved in our lattice calculations.

In addition to the Wick-contraction topologies considered above, the (3+1) topology with the single-current loop consisting of a charm propagator deserves some attention, since this contribution is neither $SU(3)_f$ nor $1/N_c$ suppressed relative to the (2+2) topology, N_c being the number of colours. In perturbation theory, the (3+1) contribution starts at $O(\alpha_s^3)$ rather than at $O(\alpha_s^2)$, while involving the same minimal number of charm propagators. Furthermore, the quark-charge and multiplicity factors numerically suppresses this contribution by a relative factor of three⁷ since it is weighted by

⁷ Within the scalar QED framework, the two topologies by themselves contain equal and opposite contributions from the D meson loops, since they cancel in $\langle \bar{c}\gamma_\mu c \bar{u}\gamma_\nu u \bar{u}\gamma_\rho u \sum_{f=u,d,s,c} \bar{q}_f \gamma_\lambda q_f \rangle$, given that the charge of D mesons is zero under the total quark number current $\sum_{f=u,d,s,c} \bar{q}_f \gamma_\lambda q_f$.

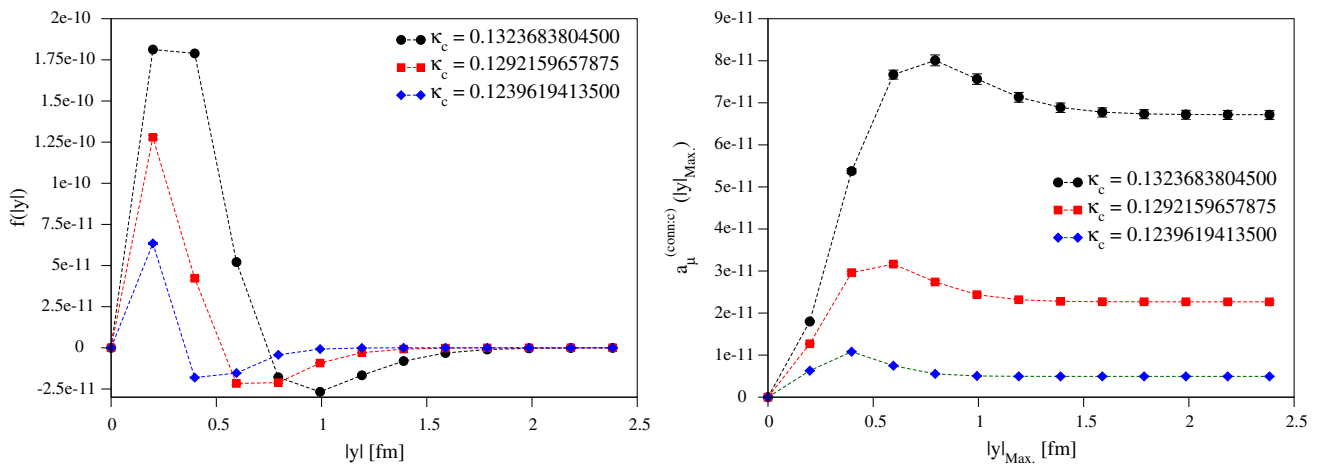


Fig. 2 The local-conserved integrands (left) and partially-integrated results (right) for a selection of κ_c s (heaviest, middle, and lightest aM_{η_c}) for our coarsest ensemble A653. Dashed lines are to guide the eye

$4 \cdot (Q_u^3 + Q_d^3 + Q_s^3)Q_c = 48/81$, while the charm–light (2+2) diagrams are weighted by 144/81, as noted above. A factor of three suppression relative to the (2+2) charm–light contribution is thus expected.

4 Lattice results for the connected contribution

As a way of validating our computational methods, our analysis has been guided by a lepton-loop calculation, much like in Ref. [27]: in Appendix A we investigate the applicability of our QED-kernel implementation at particularly heavy scales by comparing the lepton-loop contribution to a_μ^{LbL} to the known analytical expression [35]. While the agreement is acceptable at fairly heavy lepton mass, the study suggests that cut-off effects will be significant and working at unphysically-light charm mass might allow for a better handle on these effects. The physical charm mass will therefore be approached via a simultaneous extrapolation in the quark mass and in the lattice spacing.

4.1 Results at individual quark masses

For the connected part of $a_\mu^{\text{HLbL},c}$, we have performed computations with the vector current connected to the external on-shell photon (the z -vertex in Eq. (3)) being either symmetrised-conserved⁸ or local, while the rest of the currents are kept local. For each ensemble, we have tuned κ_c to get five to seven different η_c -masses, ranging from around 1.3 to 2.6 GeV. In order to better control rotational-symmetry breaking effects (and keep the higher-order lattice artifact

⁸ A definition of the local and the symmetrised-conserved current can be found for instance in Ref. [42].

coefficients the same) we will only use $f(|y|)$ along the lattice direction (1,1,1) for all ensembles.

Figure 2 shows an example of our data for the A653 ensemble. The integrand is steeply-peaked at short distances and becomes more so at heavier quark masses (smaller κ_c). As can be seen from the partially-integrated results, even the lightest charm-quark-mass lattice data used here completely saturates the integral and therefore there is no need to perform any tail-extension procedure, and just the lattice (trapezoid-rule) integral suffices. We also note that the overall integrand and integral becomes substantially smaller as κ_c decreases, representing the fact that this integral must vanish in the limit $\kappa_c \rightarrow 0$. There is a strong negative tail in the integrand causing a fairly significant cancellation for the overall integral, which becomes smaller as the charm-mass decreases. At very low κ_c on coarse lattices it is unlikely that we will be able to properly resolve the peak of the integrand and end up with a lower estimate due to the negative tail cancelling against the peak contribution more than it should. As we move to finer lattices and the resolution at low $|y|$ improves, we resolve the peak structure much better, as illustrated in Fig. 3.

4.2 Mass-dependence of the connected contribution

The results are given in Tables 3, 4, 5, 6, 7 and 8 of Appendix B and summarized in Fig. 4.

Expectations are that a_μ scales with $m_\mu^2/m_{\text{heavy}}^2$ [21–23], so it is instructive to focus on the dependence of $a_\mu^{\text{HLbL},c}$ on $1/M_{\eta_c}^2$. The data show a clear monotonic decrease as $1/M_{\eta_c}^2$ is decreased toward its physical value, starting (for the lightest charm quarks) at or above the WP prediction and ending (for the heaviest charm quarks) at or below the WP value. At similar η_c mass, the data have a large spread between the

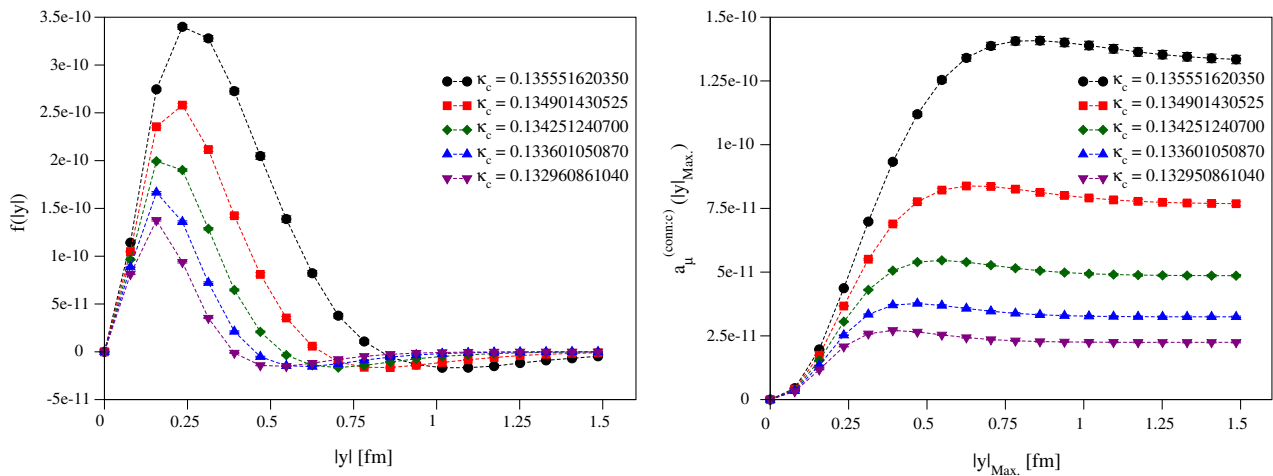


Fig. 3 The local-conserved integrands (left) and partially-integrated results (right) for all of our κ_c s, from our finest ensemble J50

coarsest and finest ensemble, indicating strong discretisation effects.

At this point, it is useful to compare the two choices of discretisations for the currents: the spread is larger in the local-local data than in the local-conserved data. Furthermore, the curvature in $1/M_{\eta_c}^2$ has a stronger dependence on the lattice spacing in the local-local data. In addition, the fact that the coarse local-local data at large M_{η_c} become negative makes it more difficult to describe the data using a fit ansatz. For these reasons, we decide to base our determination of $a_{\mu}^{\text{HLbL},c}$ solely on the analysis of the local-conserved data.

4.3 Extrapolation to the continuum and to the physical charm mass

Due to the heaviness of the valence charm quark, the intermediate states that could potentially contribute to the correlation function in question should be much suppressed at large distances; see the discussion in Sect. 3. Indeed, this can be seen by the saturation of the tail of the lattice integrand (Figs. 2, 3). For this reason, in the approach to the physical point, we assume that the finite-size effects are minor and only extrapolate in the η_c -meson mass and lattice spacing a . The statistical error on each individual data point is at the percent-level, which is comparable to the quoted error on the lattice spacings given in Table 1; therefore, it is crucial to include the error on the lattice spacing while performing an extrapolation to the physical point.

To this end, a global fit is performed based on a Bayesian approach [43], where we promote each lattice spacing to a fit-parameter and associate to it a Gaussian prior with the central value and the width taken to be the quoted central value of the lattice spacing \bar{a} and its error Δa respectively. Although the parameter space is small, constructing a fit-ansatz with a χ^2/dof on the order of unity is in fact not an easy task. After

various attempts, we have identified two classes of ansätze which are able to describe the data with reasonably good χ^2/dof .

The most restrictive constraint that we deem important to fulfill is the $m_{\mu}^2/m_{\text{heavy}}^2$ scaling of $a_{\mu}^{\text{HLbL},c}$ in the presence of a heavy scale [21–23]. It is natural to first consider the η_c -meson mass for such a scale. A challenging part of the construction of fit-ansätze is to handle the apparent non-linear behavior in $1/M_{\eta_c}^2$ of the data (see Fig. 4), which gradually gets milder as we go down in the lattice spacing. This motivates our first class of ansätze, the *P-class*, which consist of linear combinations of a leading term in $1/M_{\eta_c}^2$ and terms in $a^n f(M_{\eta_c})$ with $n \in \mathbb{N}^*$ and f an elementary function, treating the non-linearity in $1/M_{\eta_c}^2$ as a lattice artifact.

Another way to account for the $m_{\mu}^2/m_{\text{heavy}}^2$ scaling is to use the charm quark mass as a heavy scale. A rough estimate in the non-relativistic limit is that the η_c -meson mass should be equal to twice the charm quark mass, up to small relative corrections. Based on this observation, we define the *R-class* of fit ansätze, consisting of rational functions:

$$\frac{P(a, M_{\eta_c})}{\frac{1}{4}(C + M_{\eta_c})^2 + Q(a, M_{\eta_c})}, \quad (7)$$

where P and Q are polynomials in both a and M_{η_c} and C is a constant. In principle, C can also have non-trivial dependence on a and on M_{η_c} ; however, introducing additional parameters to describe this dependence turns out to be unnecessary, as the non-linearity of the data can already be well captured with the form in Eq. (7).

With the aforementioned two fit-ansatz classes, it remains nevertheless difficult to get reasonable χ^2/dof with the whole available dataset. In fact, this is not very surprising, as the resolution of the peak of the integrand becomes worse as κ_c and a become small (see Fig. 2). Therefore, it is necessary to allow for various cuts to the data. At the same time, as we

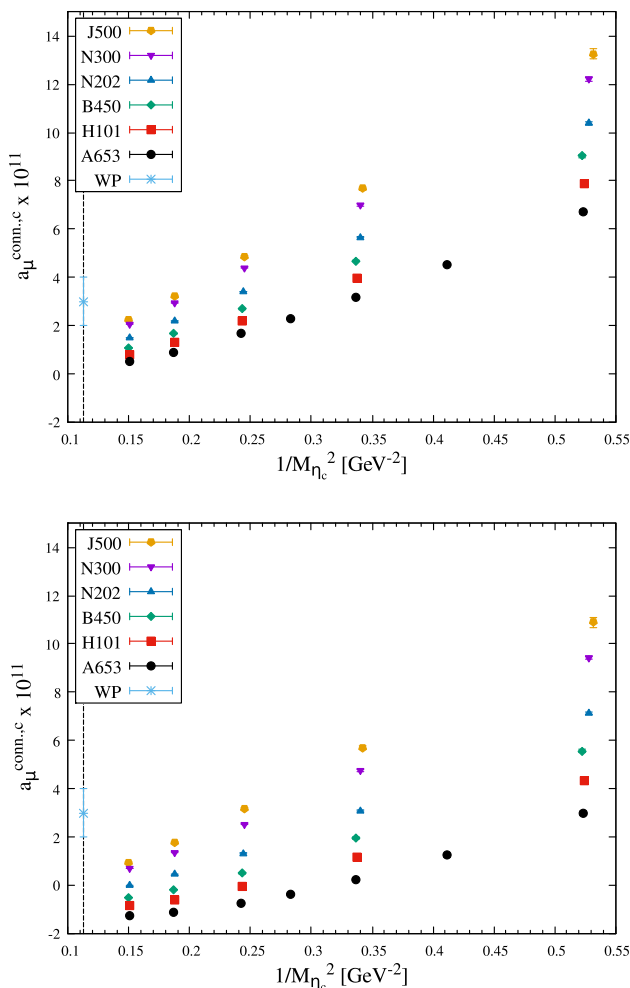


Fig. 4 Lattice results for the connected part of a_μ^{HLbL} in units of 10^{11} for the local-conserved (top) and local-local (bottom) data (see text). The black vertical line on the left indicates the physical value of $1/M_{\eta_c}^2$. The light blue point lying at physical $1/M_{\eta_c}^2$ is the estimate from Ref. [3]

would like to reach as heavy as possible M_{η_c} masses in order to have a better control over the extrapolation to its physical value, it is preferable to discard as few data points as possible. A lattice study in the pure QED case presented in App. A shows that our setup should be valid up to a charm-quark mass of at least 20/3 times that of the muon, with well-controlled cut-off effects. Based on the latter and with a simple linear relation between the physical η_c mass and the \overline{MS} -mass of the charm quark [44], we demand an admissible fit to be able to cover the data points in the range of $1/M_{\eta_c}^2 > 0.20 \text{ GeV}^{-2}$.

Our fitting strategy goes as follows: We build fit ansätze from either the P- or the R-class as explained earlier. To avoid overfitting, the number of fit parameters is limited to five. Apart from terms in $a^n M^m$, we have also tried logarithmic terms in a or M in order to allow for different types of

curvature. The four datasets we consider are (D2, D3, and D4 are defined as D1 with extra omissions):

- D1: All ensembles and data points where $1/M_{\eta_c}^2 > 0.20 \text{ GeV}^{-2}$.
- D2: D1 where data from the coarsest lattice (A653) are omitted.
- D3: D1 where the lightest M_{η_c} data of each ensemble are omitted.
- D4: D1 where $aM_{\eta_c} > 0.8$ are omitted.

Given that our final uncertainty estimate is dominated by systematics due to the choice of fit ansatz and that attempts at correlated fits yielded a poor fit quality, we choose to neglect correlations between different M_{η_c} on the same ensemble. Although this harms the statistical interpretation of χ^2 and p -values computed in the standard way, we nevertheless use these to judge relative fit quality. Our criterion for an admissible fit is one with a p -value between 0.05 and 0.95, for which the extrapolated a_μ and the p -value are stable under variation of the dataset choice.

We have tested various fit ansätze from both the P- and R-classes and found that the following five-parameter fits are able to describe our data with the quality requirements fulfilled (see Table 9 in Appendix C and Fig. 5):

$$\begin{aligned}
 \text{Fit 1: } a_\mu(a, M_{\eta_c}) &= \frac{A + BaM_{\eta_c}^2}{\frac{1}{4}(C + M_{\eta_c})^2 + (D + Ea^2M_{\eta_c}^2)^2}, \\
 \text{Fit 2: } a_\mu(a, M_{\eta_c}) &= \frac{A + BaM_{\eta_c}}{\frac{1}{4}(C + M_{\eta_c})^2 + (D + Ea^2M_{\eta_c}^2)^2}, \\
 \text{Fit 3: } a_\mu(a, M_{\eta_c}) &= \frac{A + Ba^2M_{\eta_c}^2}{\frac{1}{4}(C + M_{\eta_c})^2 + (D + EaM_{\eta_c}^2)^2}, \\
 \text{Fit 4: } a_\mu(a, M_{\eta_c}) &= Aa + \frac{B + Ca^2}{M_{\eta_c}^2} + Da^2 + E \frac{a^2}{M_{\eta_c}^4}, \\
 \text{Fit 5: } a_\mu(a, M_{\eta_c}) &= Aa + \frac{B + Ca^2}{M_{\eta_c}^2} + Da^2 + E \frac{a^2}{M_{\eta_c}^2} \ln M_{\eta_c}.
 \end{aligned} \tag{8}$$

A further important feature of these fits is that they qualitatively follow the trend of the data even in the region $1/M_{\eta_c}^2 < 0.2 \text{ GeV}^{-2}$.

As a general feature, the P-class ansätze tend to lead to larger results for $a_\mu(0, M_{\eta_c}^{\text{Phys}})$ as compared to the R-class. As there is no exclusive theoretical argument for the finite-lattice-spacing behaviour of these functions, and our data seem not to be able to unambiguously rule out any of these classes, our decision is to include the fit results with good χ^2/dof from both of them (see Table 9). More specifically, our final result is the average of our lowest (Fit 1, D3 : 2.64(4)) and our largest (Fit 5, D2 : 3.47(3)) values and we assign a generous systematic error estimate by quoting half the difference of the two, which brings us to our estimate for the

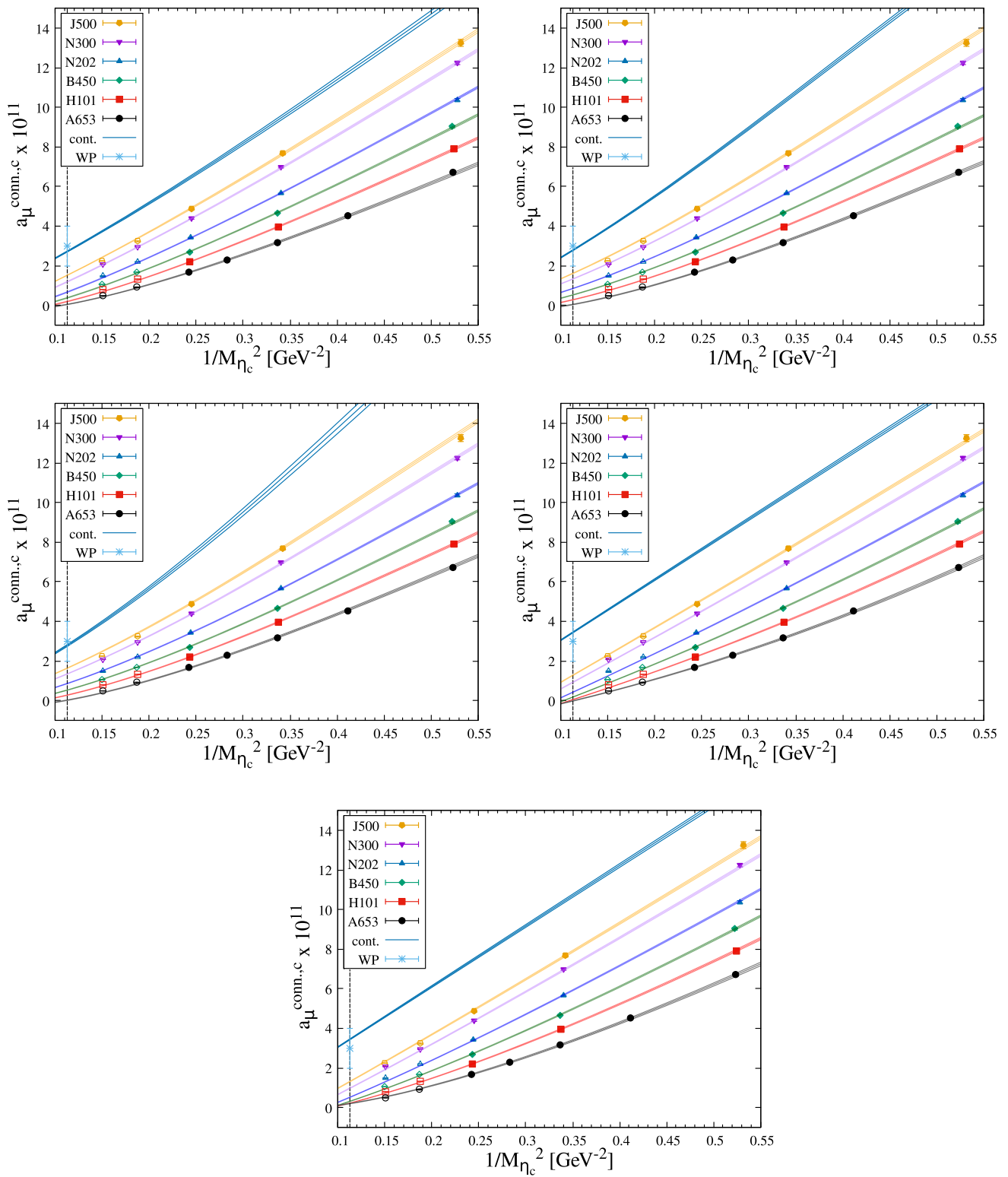


Fig. 5 Selected fit results with the dataset D1 (datapoints indicated by filled symbols): fit 1, fit 2, fit 3, fit 4, and fit 5 (left to right from the top to the bottom). The continuum limit result is given by the top-most curve (“cont.”). For other information, see Fig. 4

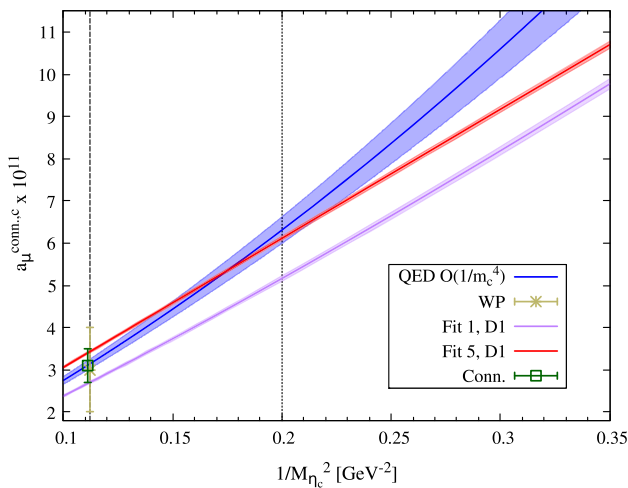


Fig. 6 The η_c -mass-dependence of $a_\mu^{\text{conn.,c}}$: comparison between our continuum-extrapolated results using Fit 1 (lower, in magenta) and Fit 5 (higher, in red) based on dataset D1 and the QED-based prediction (in blue). The band on the latter indicates a $\pm 5\%$ change in the mass-shift relating the charm-quark mass to the η_c mass (see text). The dotted vertical line indicates the upper bound for the η_c mass included in the fits. Our estimate for the connected contribution, Eq. (9), is marked with ‘Conn.’ (a horizontal offset is applied for visibility)

connected contribution,

$$a_\mu^{\text{HLbL,c,conn.}} = 3.1(4) \times 10^{-11}. \tag{9}$$

Our error on this quantity is entirely dominated by the systematic error from our modeling of its dependence on a and M_{η_c} .

4.4 Comparison to the QED-based prediction

To close the study of the connected contribution, we compare our result for $a_\mu^{\text{HLbL,c,conn.}}$ to the charm-quark loop evaluated analytically within QED as given in Eq. (5). To make contact with that expression, we need to specify the relationship between the η_c mass and the charm-quark mass. As explained while discussing the R-class of fit-ansätze, we assume the η_c mass to be twice the charm quark mass plus an almost charm-quark-mass independent mass-shift within a given window of M_{η_c} . We estimate the mass-shift using the \overline{MS} charm-quark mass and the physical M_{η_c} and assign a five-percent uncertainty to this quantity. The prediction from this prescription is displayed in Fig. 6 together with our fit results. The difference between truncating at $O(1/m_c^2)$ and at $O(1/m_c^4)$ is tiny compared to the uncertainty that we assign to the mass-shift inferred from our prescription. It is worth noting that, even though the QED-based prediction gives a result that falls in the bulk of our estimate Eq. (9) at the physical charm mass, the milder curvatures in $1/M_{\eta_c}^2$ of the representative fit results suggest that non-perturbative effects are still significant at intermediate masses.

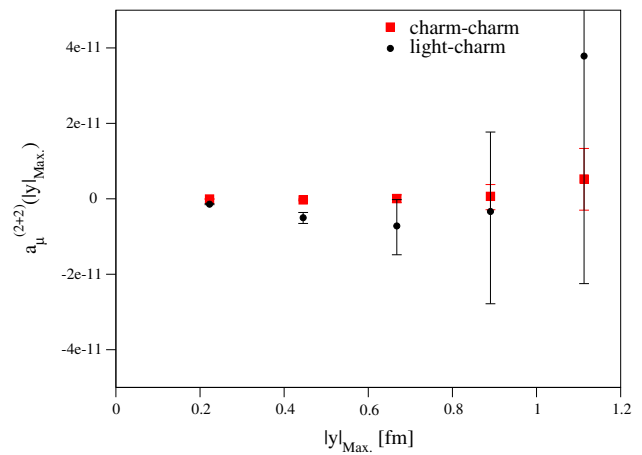


Fig. 7 The (2+2) charm–light and charm–charm partially-integrated data for ensemble N202

5 The disconnected contribution

The disconnected parts of the charm contribution are expected to be very small. From the outset, we neglect the (3+1), (2+1+1), and (1+1+1+1) Wick-contraction topologies, based partly on them being consistent with zero for the light quark contribution, as found in [20], and partly on the arguments laid out in Sect. 3. This leaves us with the (2+2) topology, which is a sizeable contribution in the light-quark a_μ^{HLbL} result. This contribution can be broken into the mixed charm–light and the charm–charm contributions, with the former (by analogy with the strange sector) expected to be the major contribution.

As the disconnected contribution is still an expensive calculation, we have limited ourselves to a single charm-quark mass determined by κ_c from the D_s -tuning of Ref. [30]. This tuning is suboptimal for our present purposes, an aspect we return to below. We will also use the Z_V^c values from [30], except for ensemble A653, where we computed the renormalisation factor ourselves. We employ exclusively local vector currents and restrict ourselves to the ensembles N300, N202, B450, and A653, reusing data for the light-quark loop from Ref. [27].

A plot of the partially-integrated charm–light and charm–charm disconnected contributions for ensemble N202 is shown in Fig. 7. It is clear that both of these contributions are noisy, small, negative, and very short-distance. Again this means we can use the lattice integral directly for our final result, and we use a simple constant fit to the partially-integrated result for our final determination. Based on the numerical evidence from Figs. 2, 3 that the connected contribution becomes very short-ranged as the charm mass is increased towards its physical value, as well as the theoretical arguments of Sect. 3, we start this fit between 0.4 and 0.5 fm. Table 2 shows our results for this procedure and

Table 2 The charm–light and charm–charm (2+2) contributions to a_μ^{HLbL}

Ensemble	κ_c	Z_V^c	$a_\mu^{2+2;lc} \times 10^{11}$	$a_\mu^{2+2;cc} \times 10^{11}$
A653	0.119759	1.32265	−3.24(99)	−0.06(2)
B450	0.125095	1.12972	−0.53(27)	+0.01(2)
N202	0.127579	1.04843	−0.48(14)	−0.03(2)
N300	0.130099	0.97722	−0.39(8)	−0.03(1)

we see that A653 is an extreme outlier in the charm–light contribution. The other, finer, ensembles yield values much smaller and consistent with one another. We decide to omit this coarse ensemble entirely and fit the remaining charm–light data to a straight line in the variable a^2 . This leads to the result $a_\mu^{\text{HLbL},c,(2+2)} = -0.28(21) \times 10^{-11}$.

We now come back to the issue of the tuning of the charm quark mass. The CLS ensembles we are using are designed to have the trace of the quark mass matrix equal to its physical value, to a rather good approximation [29]. We remind the reader that for the connected contribution, we chose the charm–quark mass such that the physical η_c mass is reproduced. With this choice, the dependence of charm correlators on the $SU(3)_f$ breaking parameter $[m_s - (m_u + m_d)/2]$ is expected to be small, being a pure sea quark effect. As a consequence, the extrapolation to physical (u, d, s) quark masses is expected to be very mild. This is not the case if we tune the mass \bar{M}_D of the triplet of D mesons at our $SU(3)_f$ -symmetric point to the physical D_s meson, $M_{D_s} = 1.968$ GeV. By contrast, if we tune \bar{M}_D to the average $(\bar{M}_D)_{\text{phys}} \equiv \frac{1}{3}[M_{D^+} + M_{D^0} + M_{D_s}]_{\text{phys}} = 1.901$ GeV of the physical D meson masses, then we again avoid a valence–quark effect in the approach to physical quark masses. It is also interesting to ask, how different a tuning this represents as compared to the tuning via the η_c mesons mass. We have found that the η_c meson mass, extrapolated to the charm mass where $\bar{M}_D = (\bar{M}_D)_{\text{phys}}$, amounts to 2.97(4) GeV, which is consistent with its physical value. This is an indication that sea quark effects are indeed small in the charm sector.

These observations lead us to apply a small correction to the charm–light disconnected contribution, to bring it to the point where \bar{M}_D takes the value $(\bar{M}_D)_{\text{phys}}$. Assuming that the disconnected contribution is roughly proportional to $1/\bar{M}_D^2$, we multiply our continuum-extrapolated result obtained at $\bar{M}_D = M_{D_s}$ with the ratio $(M_{D_s}/\bar{M}_D)_{\text{phys}}^2$, leading to the final result

$$a_\mu^{\text{HLbL},c,(2+2)} = -0.30(23) \times 10^{-11}. \quad (10)$$

We neglect the charm–charm contribution as its contribution is far smaller than our final error for the charm–light.

6 Discussion of the results and conclusion

We have determined the charm–quark contribution to hadronic light-by-light scattering in the anomalous magnetic moment of the muon. We find that the lattice determination of this quantity is challenging, specifically in the modeling of the connected contribution’s discretisation effects: the associated systematic error dominates our final error budget. As expected from the charm–loop picture, the connected contribution turns out to be the most significant overall. We find the charm–light disconnected contribution to be negative and much smaller in magnitude than the fully-connected contribution, amounting to a 10% correction with a large uncertainty. The charm–charm disconnected contribution is entirely negligible and we expect all higher-order contributions to be equally insignificant.

Before quoting our final result for the charm contribution to a_μ^{HLbL} , we address the question of its dependence on the (u, d, s) quark masses. The fact that several aspects of our lattice results can be understood via the charm–quark loop picture is an indication that this dependence must be modest, and we may attempt to estimate its order of magnitude via the ambiguity induced by the choice of the charm–quark tuning condition away from the physical (u, d, s) quark-mass point. We saw in Sect. 5 that tuning the average D^+ , D^0 and D_s mass to its physical value was equivalent, within our uncertainties, to tuning the η_c mass to its physical value. Still, we estimate that the connected contribution would potentially be modified by 2% had we chosen the alternative tuning. Another estimate can be based on the idea that the charm contribution is proportional to the sum of the inverses of the charged D -meson squared masses. That sum differs again by about two percent from the square inverse of the average D^+ , D^0 and D_s mass. This argument suggests an absolute systematic error of 0.06×10^{-11} , which we conservatively inflate to 0.12×10^{-11} and add in quadrature to the other uncertainties below. This estimate also covers the (u, d, s) valence–quark mass dependence present in the charm–light disconnected contribution: as discussed in Sect. 3, for that topology we expect a short-range contribution (with a reach of order $(2m_c)^{-1}$), plus a longer-range contribution with a very suppressed amplitude coming from the exchange of (u, d, s) isoscalar mesons. The short-range part is again expected to depend on the light–quark masses mainly via the D meson

masses as estimated above, while the longer-ranger part is simply too small to affect our estimate.

Our full result from adding Eqs. (9) and (10) together and adding errors in quadrature is

$$a_{\mu}^{\text{HLbL,c}} = (2.8 \pm 0.5) \times 10^{-11}. \quad (11)$$

This result is completely consistent with the 2020 White Paper estimate of $(3 \pm 1) \times 10^{-11}$ [3], and has half its uncertainty.

Combining Eq. (11) with our previous result from the light and strange contributions of $a_{\mu}^{\text{HLbL,ls}} = (106.8 \pm 15.9) \times 10^{-11}$ [20] obtained with dynamical (u, d, s) quarks yields a fully non-perturbative determination of a_{μ}^{HLbL} , including all relevant contributions. A last effect not yet accounted for is the charm sea-quark effect on the light-quark contributions, as for instance the D^+ meson loop can contribute to the connected four-point function of the down quark in a calculation with dynamical (u, d, s, c) quarks. Within a scalar-QED treatment of the D meson, we have however estimated this effect to be below 0.1×10^{-11} . Therefore we neglect the charm sea quark effects and arrive at

$$a_{\mu}^{\text{HLbL}} = (109.6 \pm 15.9) \times 10^{-11}. \quad (12)$$

This concludes our first-generation calculation of hadronic light-by-light scattering in the muon ($g - 2$).

Acknowledgements We thank Andreas Nyffeler for a fruitful collaboration on computing the QED kernel used here. This work is supported by the European Research Council (ERC) under the European Union's Horizon 2020 research and innovation programme through grant agreement 771971-SIMDAMA, and through the Cluster of Excellence *Precision Physics, Fundamental Interactions, and Structure of Matter* (PRISMA+ EXC 2118/1) within the German Excellence Strategy (Project ID 39083149). The project leading to this publication has also received funding from the Excellence Initiative of Aix-Marseille University – A*MIDEX, a French “Investissements d’Avenir” programme, AMX-18-ACE-005. JRG acknowledges support from the Simons Foundation through the Simons Bridge for Postdoctoral Fellowships scheme. Calculations for this project were performed on the HPC clusters “Clover” and “HIMster II” at the Helmholtz-Institut Mainz and “Mogon II” at JGU Mainz. Our programs use the deflated SAP+GCR solver from the openQCD package [45], as well as the QDP++ library [46]. We are grateful to our colleagues in the CLS initiative for sharing ensembles.

Data Availability Statement This manuscript has no associated data or the data will not be deposited. [Authors' comment: The paper itself contains many intermediate results collected in tables.]

Open Access This article is licensed under a Creative Commons Attribution 4.0 International License, which permits use, sharing, adaptation, distribution and reproduction in any medium or format, as long as you give appropriate credit to the original author(s) and the source, provide a link to the Creative Commons licence, and indicate if changes were made. The images or other third party material in this article are included in the article's Creative Commons licence, unless indicated otherwise in a credit line to the material. If material is not included in the article's Creative Commons licence and your intended use is not permitted by statutory regulation or exceeds the permit-

ted use, you will need to obtain permission directly from the copyright holder. To view a copy of this licence, visit <http://creativecommons.org/licenses/by/4.0/>.

Funded by SCOAP³. SCOAP³ supports the goals of the International Year of Basic Sciences for Sustainable Development.

Appendix A: Methodology test for a heavy lepton

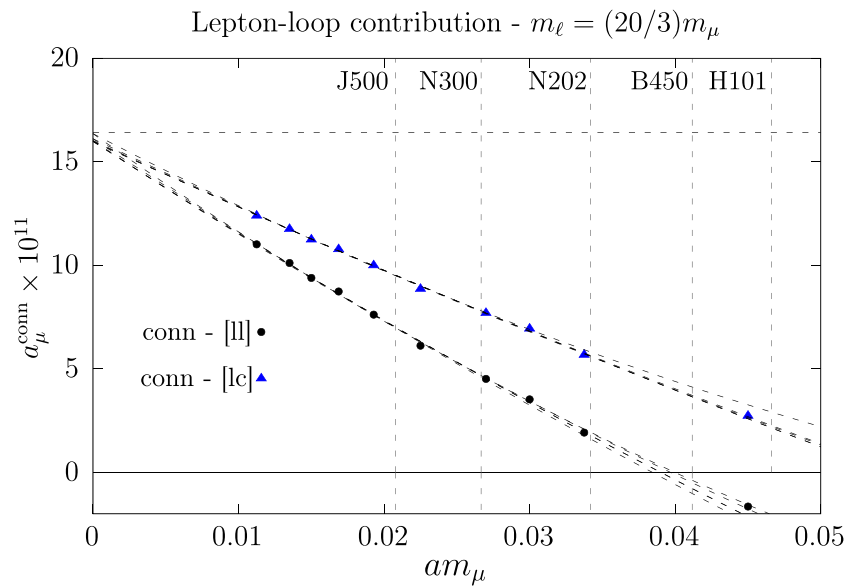
With our implementation of the QED coordinate-space kernel, we have been able to reproduce various known light-by-light contributions in the continuum [27,47,48] at the one-percent level. The tests performed so far concern physics involving particles with masses on the same order as the muon mass. As our implementation of the QED-kernel relies on interpolating weight functions that are precomputed on a grid [34], it is important for the goal of this paper to test how robust this implementation is for computing contributions from more massive particles (Fig. 8).

As an example of a calculation performed entirely in the continuum, we quote the result we obtain with the kernel $\tilde{\mathcal{L}}^{(\Lambda=0.40)}$ and ‘method 2’ for the lepton-loop contribution with $m_{\ell}/m_{\mu} = 4$, namely $a_{\mu}^{\text{HLbL}} = (42.1 \pm 0.5) \times 10^{-11}$; the exact result is $(43.175\dots) \times 10^{-11}$. While this precision is sufficient for our present purposes, it is clear that, using continuum propagators for the lepton loop, the quality and stability of the coordinate-space results degrade when the lepton mass increases.⁹

In order to validate our computational setup, we turn to a test that is much closer to the procedure we used for the charm-quark contribution in lattice QCD. We have computed the lepton-loop contribution to a_{μ}^{HLbL} using lattice fermion propagators at a mass-scale relevant for this project, choosing specifically $m_{\ell}/m_{\mu} = 20/3$. We proceed by repeating the calculation on increasingly fine lattices and perform a continuum extrapolation using a quadratic polynomial in am_{μ} . Here, two discretisations of the vector current at the external vertex z were used, and the resulting contributions to a_{μ}^{LbL} were extrapolated simultaneously to the continuum, enforcing a common continuum value. The deviation of the continuum-extrapolated result from the known exact result of $16.395\dots \times 10^{-11}$ depends somewhat on the choice of the extrapolation range, but is in all cases within 2.5%. This successfully passed test gives us confidence that the setup used for the lattice-QCD calculation presented in the main text is robust for fermion masses up to at least 700 MeV.

⁹ In our estimate, we regulate the numerics by setting the integrand to zero when two vertices come within a distance of $10^{-3}m_{\mu}^{-1}$. A more sophisticated procedure should be used for higher lepton masses.

Fig. 8 Continuum extrapolation for the lepton loop with $m_\ell/m_\mu = 20/3$, computed on the lattice with two discretisations of the vector current (local or conserved) at the external vertex z



Appendix B: Tables of data for the connected contribution

using the ‘local-local’ [ll] and ‘local-conserved’ [lc] discretisations.

This appendix contains the Tables 3 through 8 providing the results for the connected charm contribution to a_μ^{HLbL} ,

Table 3 Results for ensemble A653, a_μ has been multiplied by 10^{11}

κ_c	M_{η_c} [GeV]	$Z_V^{(c)}$	$a_\mu^{(\text{Conn.}[lc])}$	$a_\mu^{(\text{Conn.}[ll])}$
0.1239619413500	2.5780	1.15128(7)	0.494(9)	-1.246(26)
0.1260635511250	2.3144	1.06998(7)	0.909(13)	-1.110(33)
0.1281651609000	2.0316	0.99145(6)	1.657(23)	-0.726(42)
0.1292159657875	1.8815	0.95307(6)	2.268(31)	-0.359(48)
0.1302667706750	1.7243	0.91530(6)	3.163(44)	0.238(58)
0.1313175755625	1.5589	0.87813(6)	4.527(61)	1.236(73)
0.1323683804500	1.3827	0.84154(9)	6.717(106)	2.973(101)

Table 4 Same as Table 3 but for ensemble H101

κ_c	M_{η_c} [GeV]	$Z_V^{(c)}$	$a_\mu^{(\text{Conn.}[lc])}$	$a_\mu^{(\text{Conn.}[ll])}$
0.1263626550	2.5764	1.07159(7)	0.811(7)	-0.827(15)
0.1280954825	2.3112	1.00793(7)	1.313(10)	-0.588(19)
0.1298283100	2.0282	0.94610(6)	2.205(16)	-0.059(25)
0.1315611375	1.7212	0.88580(7)	3.952(21)	1.168(36)
0.1332939650	1.3811	0.82708(6)	7.901(69)	4.328(70)

Table 5 Same as Table 3 but for ensemble B450

κ_c	M_{η_c} [GeV]	$Z_V^{(c)}$	$a_\mu^{(\text{Conn.}[lc])}$	$a_\mu^{(\text{Conn.}[ll])}$
0.128043750	2.5817	1.02163(4)	1.073(7)	-0.521(14)
0.129517875	2.3144	0.96948(3)	1.663(10)	-0.190(18)
0.13092500	2.0298	0.91842(3)	2.696(17)	0.488(22)
0.132466875	1.7228	0.86851(3)	4.676(30)	1.963(34)
0.133941250	1.3830	0.81977(4)	9.037(65)	5.558(65)

Table 6 Same as Table 3 but for ensemble N202

κ_c	M_{η_c} [GeV]	$Z_V^{(c)}$	$a_\mu^{(\text{Conn.}[lc])}$	$a_\mu^{(\text{Conn.}[ll])}$
0.129934250	2.5763	9.68482(3)	1.483(7)	-0.021(10)
0.131111875	2.3077	0.92860(3)	2.199(10)	0.444(12)
0.132289500	2.0227	0.88955(6)	3.409(16)	1.322(16)
0.133467125	1.7154	0.85096(2)	5.650(28)	3.094(26)
0.134644750	1.3760	0.81322(2)	10.381(55)	7.115(55)

Table 7 Same as Table 3 but for ensemble N300

κ_c	M_{η_c} [GeV]	$Z_V^{(c)}$	$a_\mu^{(\text{Conn.}[lc])}$	$a_\mu^{(\text{Conn.}[ll])}$
0.131824250	2.5779	0.92043(8)	2.066(12)	0.695(15)
0.132686875	2.3074	0.89253(4)	2.943(17)	1.361(19)
0.133549500	2.0209	0.86506(3)	4.390(27)	2.529(28)
0.134412125	1.7137	0.83794(3)	6.980(47)	4.733(44)
0.135274750	1.3763	0.81118(3)	12.236(95)	9.425(81)

Table 8 Same as Table 3 but for ensemble J500

κ_c	M_{η_c} [GeV]	$Z_V^{(c)}$	$a_\mu^{(\text{Conn.}[lc])}$	$a_\mu^{(\text{Conn.}[ll])}$
0.132950861040	2.5849	0.89274(1)	2.245(19)	0.950(20)
0.133601050870	2.3090	0.87241(1)	3.239(27)	1.781(28)
0.134251240700	2.0194	0.85228(1)	4.860(45)	3.183(43)
0.134901430525	1.7102	0.83240(4)	7.686(77)	5.707(74)
0.135551620350	1.3718	0.81266(1)	13.255(196)	10.890(197)

Appendix C: Fit results for the connected contribution

In this appendix we collect details of the fit results to the local-conserved connected data obtained with the fit ansätze of Eq. (8). The values obtained for $a_\mu^{\text{HLbL},c,\text{conn.}}$, as well as the corresponding χ^2/dof and p values are given in Table 9.

Table 9 Fit results of the local-conserved connected charm contribution to a_μ

Fit	Dataset	$a_\mu^{\text{HLbL},c,\text{conn.}} \times 10^{11}$	χ^2/dof	p -value
Fit1	D1	2.71(3)	1.08	0.37
Fit1	D2	2.71(3)	1.18	0.30
Fit1	D3	2.64(4)	1.07	0.38
Fit1	D4	2.76(3)	1.27	0.23
Fit2	D1	2.77(3)	1.11	0.34
Fit2	D2	2.81(3)	1.37	0.19
Fit2	D3	2.72(3)	1.14	0.33
Fit2	D4	2.85(3)	1.03	0.42
Fit3	D1	2.77(5)	1.59	0.07
Fit3	D2	2.72(5)	1.98	0.03
Fit3	D3	2.84(4)	1.74	0.07
Fit3	D4	2.66(5)	1.18	0.30

Table 9 continued

Fit	Dataset	$a_\mu^{\text{HLbL},c,\text{conn.}} \times 10^{11}$	χ^2/dof	p -value
Fit4	D1	3.43(3)	1.51	0.09
Fit4	D2	3.47(3)	1.48	0.14
Fit4	D3	3.43(3)	1.90	0.05
Fit4	D4	3.45(3)	1.97	0.03
Fit5	D1	3.43(3)	1.48	0.10
Fit5	D2	3.47(3)	1.48	0.14
Fit5	D3	3.42(3)	1.92	0.04
Fit5	D4	3.45(3)	1.94	0.03

References

1. B. Abi et al. (Muon g-2), Measurement of the positive muon anomalous magnetic moment to 0.46 ppm. Phys. Rev. Lett. **126**, 141801 (2021). [arXiv:2104.03281](https://arxiv.org/abs/2104.03281) [hep-ex]
2. G.W. Bennett et al. (Muon (g - 2)), Final report of the E821 muon anomalous magnetic moment measurement at BNL. Phys. Rev. D **73**, 072003 (2006). [arXiv:hep-ex/0602035](https://arxiv.org/abs/hep-ex/0602035)
3. T. Aoyama et al., The anomalous magnetic moment of the muon in the Standard Model. Phys. Rep. **887**, 1 (2020). [arXiv:2006.04822](https://arxiv.org/abs/2006.04822) [hep-ph]
4. S. Borsanyi et al., Leading hadronic contribution to the muon magnetic moment from lattice QCD. Nature **593**, 51 (2021). [arXiv:2002.12347](https://arxiv.org/abs/2002.12347) [hep-lat]

5. G. Colangelo, M. Hoferichter, M. Procura, P. Stoffer, Dispersion relation for hadronic light-by-light scattering: theoretical foundations. *JHEP* **09**, 074 (2015). [arXiv:1506.01386](#) [hep-ph]
6. K. Melnikov, A. Vainshtein, Hadronic light-by-light scattering contribution to the muon anomalous magnetic moment revisited. *Phys. Rev. D* **70**, 113006 (2004). [arXiv:hep-ph/0312226](#)
7. P. Masjuan, P. Sánchez-Puertas, Pseudoscalar-pole contribution to the $(g_\mu - 2)$: a rational approach. *Phys. Rev. D* **95**, 054026 (2017). [arXiv:1701.05829](#) [hep-ph]
8. G. Colangelo, M. Hoferichter, M. Procura, P. Stoffer, Dispersion relation for hadronic light-by-light scattering: two-pion contributions. *JHEP* **04**, 161 (2017). [arXiv:1702.07347](#) [hep-ph]
9. M. Hoferichter, B.-L. Hoid, B. Kubis, S. Leupold, S.P. Schneider, Dispersion relation for hadronic light-by-light scattering: pion pole. *JHEP* **10**, 141 (2018). [arXiv:1808.04823](#) [hep-ph]
10. A. Gérardin, H.B. Meyer, A. Nyffeler, Lattice calculation of the pion transition form factor with $N_f = 2 + 1$ Wilson quarks. *Phys. Rev. D* **100**, 034520 (2019). [arXiv:1903.09471](#) [hep-lat]
11. J. Bijnens, N. Hermansson-Truedsson, A. Rodríguez-Sánchez, Short-distance constraints for the HLbL contribution to the muon anomalous magnetic moment. *Phys. Lett. B* **798**, 134994 (2019). [arXiv:1908.03331](#) [hep-ph]
12. G. Colangelo, F. Hagelstein, M. Hoferichter, L. Laub, P. Stoffer, Longitudinal short-distance constraints for the hadronic light-by-light contribution to $(g - 2)_\mu$ with large- N_c Regge models. *JHEP* **03**, 101 (2020). [arXiv:1910.13432](#) [hep-ph]
13. V. Pauk, M. Vanderhaeghen, Single meson contributions to the muon's anomalous magnetic moment. *Eur. Phys. J. C* **74**, 3008 (2014). [arXiv:1401.0832](#) [hep-ph]
14. I. Danilkin, M. Vanderhaeghen, Light-by-light scattering sum rules in light of new data. *Phys. Rev. D* **95**, 014019 (2017). [arXiv:1611.04646](#) [hep-ph]
15. F. Jegerlehner, *The anomalous magnetic moment of the muon*, vol. 274 (Springer, Cham, 2017)
16. M. Knecht, S. Narison, A. Rabemananjara, D. Rabetiariovony, Scalar meson contributions to a_μ from hadronic light-by-light scattering. *Phys. Lett. B* **787**, 111 (2018). [arXiv:1808.03848](#) [hep-ph]
17. G. Eichmann, C.S. Fischer, R. Williams, Kaon-box contribution to the anomalous magnetic moment of the muon. *Phys. Rev. D* **101**, 054015 (2020). [arXiv:1910.06795](#) [hep-ph]
18. P. Roig, P. Sánchez-Puertas, Axial-vector exchange contribution to the hadronic light-by-light piece of the muon anomalous magnetic moment. *Phys. Rev. D* **101**, 074019 (2020). [arXiv:1910.02881](#) [hep-ph]
19. T. Blum, N. Christ, M. Hayakawa, T. Izubuchi, L. Jin, C. Jung, C. Lehner, Hadronic light-by-light scattering contribution to the muon anomalous magnetic moment from lattice QCD. *Phys. Rev. Lett.* **124**, 132002 (2020). [arXiv:1911.08123](#) [hep-lat]
20. E.-H. Chao, R.J. Hudspith, A. Gérardin, J.R. Green, H.B. Meyer, K. Ottnad, Hadronic light-by-light contribution to $(g - 2)_\mu$ from lattice QCD: a complete calculation. *Eur. Phys. J. C* **81**, 651 (2021). [arXiv:2104.02632](#) [hep-lat]
21. V.B. Berestetskii, O.N. Krokhn, A.K. Khlebnikov, Concerning the radiative correction to the μ -meson magnetic moment. *JETP* **3**, 761 (1956)
22. V.B. Berestetskii, O.N. Krokhn, A.K. Khlebnikov, *Zh. Eksp. Teor. Fiz.* **30**, 788 (1956)
23. W.S. Cowland, On Schwinger's theory of the muon. *Nucl. Phys.* **8**, 397 (1958)
24. J. Prades, E. de Rafael, A. Vainshtein, The hadronic light-by-light scattering contribution to the muon and electron anomalous magnetic moments. *Adv. Ser. Direct. High Energy Phys.* **20**, 303 (2009). [arXiv:0901.0306](#) [hep-ph]
25. J. Bijnens, N. Hermansson-Truedsson, L. Laub, A. Rodríguez-Sánchez, The two-loop perturbative correction to the $(g - 2)_\mu$ HLbL at short distances. *JHEP* **04**, 240 (2021). [arXiv:2101.09169](#) [hep-ph]
26. J. Bijnens, J. Releforts, Pion light-by-light contributions to the muon $g - 2$. *JHEP* **09**, 113 (2016). [arXiv:1608.01454](#) [hep-ph]
27. E.-H. Chao, A. Gérardin, J.R. Green, R.J. Hudspith, H.B. Meyer, Hadronic light-by-light contribution to $(g - 2)_\mu$ from lattice QCD with SU(3) flavor symmetry. *Eur. Phys. J. C* **80**, 869 (2020). [arXiv:2006.16224](#) [hep-lat]
28. M. Bruno et al., Simulation of QCD with $N_f = 2 + 1$ flavors of non-perturbatively improved Wilson fermions. *JHEP* **02**, 043 (2015). [arXiv:1411.3982](#) [hep-lat]
29. M. Bruno, T. Korzec, S. Schaefer, Setting the scale for the CLS $2 + 1$ flavor ensembles. *Phys. Rev. D* **95**, 074504 (2017). [arXiv:1608.08900](#) [hep-lat]
30. A. Gérardin, M. Cè, G. von Hippel, B. Hörz, H.B. Meyer, D. Mohler, K. Ottnad, J. Wilhelm, H. Wittig, The leading hadronic contribution to $(g - 2)_\mu$ from lattice QCD with $N_f = 2 + 1$ flavours of $O(a)$ improved Wilson quarks. *Phys. Rev. D* **100**, 014510 (2019). [arXiv:1904.03120](#) [hep-lat]
31. R.J. Hudspith, D. Mohler, A fully non-perturbative charm-quark tuning using machine learning (2021). [arXiv:2112.01997](#) [hep-lat]
32. M. Foster, C. Michael (UKQCD), Quark mass dependence of hadron masses from lattice QCD. *Phys. Rev. D* **59**, 074503 (1999). [arXiv:hep-lat/9810021](#)
33. P.A. Boyle, C. Kelly, R.D. Kenway, A. Jüttner, Use of stochastic sources for the lattice determination of light quark physics. *JHEP* **08**, 086 (2008). [arXiv:0804.1501](#) [hep-lat]
34. N. Asmussen, J. Green, H.B. Meyer, A. Nyffeler, Position-space approach to hadronic light-by-light scattering in the muon $g - 2$ on the lattice. *PoS LATTICE2016*, 164 (2016). [arXiv:1609.08454](#) [hep-lat]
35. S. Laporta, E. Remiddi, The analytical value of the electron light-light graphs contribution to the muon $(g - 2)$ in QED. *Phys. Lett. B* **301**, 440 (1993)
36. J.H. Kuhn, A.I. Onishchenko, A.A. Pivovarov, O.L. Veretin, Heavy mass expansion, light by light scattering and the anomalous magnetic moment of the muon. *Phys. Rev. D* **68**, 033018 (2003). [arXiv:hep-ph/0301151](#)
37. W. Heisenberg, H. Euler, Consequences of Dirac's theory of positrons. *Z. Phys.* **98**, 714 (1936). [arXiv:physics/0605038](#)
38. V.A. Novikov, M.A. Shifman, A.I. Vainshtein, V.I. Zakharov, In search of scalar gluonium. *Nucl. Phys. B* **165**, 67 (1980)
39. V.A. Novikov, M.A. Shifman, A.I. Vainshtein, V.I. Zakharov, A theory of the $J/\psi \rightarrow \eta(\eta')\gamma$ decays. *Nucl. Phys. B* **165**, 55 (1980)
40. A. Nyffeler, Precision of a data-driven estimate of hadronic light-by-light scattering in the muon $g - 2$: pseudoscalar-pole contribution. *Phys. Rev. D* **94**, 053006 (2016). [arXiv:1602.03398](#) [hep-ph]
41. M. Knecht, A. Nyffeler, M. Perrottet, E. de Rafael, Hadronic light by light scattering contribution to the muon $g - 2$: an effective field theory approach. *Phys. Rev. Lett.* **88**, 071802 (2002). [arXiv:hep-ph/0111059](#)
42. A. Gérardin, T. Harris, H.B. Meyer, Nonperturbative renormalization and $O(a)$ -improvement of the nonsinglet vector current with $N_f = 2 + 1$ Wilson fermions and tree-level Symanzik improved gauge action. *Phys. Rev. D* **99**, 014519 (2019). [arXiv:1811.08209](#) [hep-lat]
43. G.P. Lepage, B. Clark, C.T.H. Davies, K. Hornbostel, P.B. Mackenzie, C. Morningstar, H. Trotter, Constrained curve fitting. *Nucl. Phys. B Proc. Suppl.* **106**, 12 (2002). [arXiv:hep-lat/0110175](#)
44. P. Zyla et al. (Particle Data Group), Review of particle physics. *PTEP* **2020**, 083C01 (2020)
45. M. Lüscher, S. Schaefer, Lattice QCD with open boundary conditions and twisted-mass reweighting. *Comput. Phys. Commun.* **184**, 519 (2013). [arXiv:1206.2809](#) [hep-lat]
46. R.G. Edwards, B. Joó (SciDAC, LHPC, UKQCD), The Chroma software system for lattice QCD, *Lattice field theory. Proceed-*

- ings, 22nd international symposium, Lattice 2004, Batavia, USA, June 21–26, 2004*. Nucl. Phys. B (Proc. Suppl.) **140**, 832 (2005). [arXiv:hep-lat/0409003](#)
47. N. Asmussen, E.-H. Chao, A. Gérardin, J.R. Green, R.J. Hudspith, H.B. Meyer, A. Nyffeler, Developments in the position-space approach to the HLbL contribution to the muon $g - 2$ on the lattice, in *Proceedings 37th international symposium on lattice field theory (lattice 2019), Wuhan, China, 16–22 June 2019*. PoS **LATTICE2019**, 195 (2019). [arXiv:1911.05573](#) [hep-lat]
48. N. Asmussen, A. Gérardin, H.B. Meyer, A. Nyffeler, Exploratory studies for the position-space approach to hadronic light-by-light scattering in the muon $g - 2$. EPJ Web Conf. **175**, 06023 (2018). [arXiv:1711.02466](#) [hep-lat]